J. Ocean Univ. China (Oceanic and Coastal Sea Research)
DOI 10.1007/s11802-016-2721-6
ISSN 1672-5182, 2016 15 (2): 201-208
http://www.ouc.edu.cn/xbywb/
E-mail:xbywb@ouc.edu.cn

Tide and Current Observations in the Central Chukchi Sea During the Summer of 2012

WANG Huiwu[1), 2)], LIU Na[2), *], and CHEN Hongxia[2)]

1) *College of Physical and Environmental Oceanography*, *Ocean University of China*, *Qingdao* 266100, *P. R. China*
2) *First Institute of Oceanography*, *State Oceanic Administration*, *Qingdao* 266061, *P. R. China*

(Received July 31, 2014; revised October 13, 2014; accepted December 14, 2015)

Abstract Current data from a moored Acoustic Doppler Current Profiler (ADCP) deployed at 69°30.155′N, 169°00.654′W in the central Chukchi Sea during 2012 summertime is analyzed in the present paper. Characteristics of tidal and residual currents are obtained with Cosine-Lanczos filter and cross-spectral analyses. The main achievements are as follows: 1) Along with the local inertial frequency of 12.8 h, two other peaks at ~12-h and ~10-d dominate the time series of raw velocity; 2) The M_2 dominates the 6 resolved tide constituents with significant amplitude variations over depth and the ratios of current speed of this constituent to that of the total tidal current are 54% and 47% for *u* and *v* components, respectively. All the resolved tidal constituents rotate clockwise at depth with the exception of MM and O_1. The constituents of M_2 and S_2 with the largest major semi-axes are similar in eccentricity and orientation at deeper levels; 3) The maximum of residual currents varies in a range of 20–30 cm s^{-1} over depth and the current with lower velocities flow more true north with smaller magnitudes compared to the current in surface layer. The ~10 d fluctuation of residual current is found throughout the water column and attributed to the response of current to the local wind forcing, with an approximate 1.4 d lag-time at the surface level and occurring several hours later in the lower layer; 4) Mean residual currents flow toward the north with the magnitudes smaller than 7 cm s^{-1} in a general agreement with previous studies, which suggests a relatively weaker but stable northward flow indeed exists in the central Chukchi Sea.

Key words central Chukchi Sea; tidal and residual currents; local wind forcing

1 Introduction

As the unique Arctic marginal sea with its extensive continental shelf (~800 km) and relatively shallow depth (~50 m), the Chukchi Sea connects the Arctic and the Bering Strait through several pathways via which the Pacific-origin waters enter to influence the freshwater balance, heat, and water movement and exchanges with the Arctic Ocean (Woodgate *et al*., 2005).

Driven by the sea-level difference between the Pacific and Arctic Oceans (Coachman and Aagaard, 1966), a ~0.8 Sv of the Pacific waters (Roach *et al*., 1995) is suggested entering the Chukchi Sea. With a significant transit time ranging from one to six months (Woodgate *et al*., 2005), the Pacific inflow remarkably modifies the dynamics processes, the ice extent, and ecosystem of the productive Chukchi Sea (Walsh *et al*., 1989; Arrigo *et al*., 2014; Hunt *et al*., 2013).

It was broadly believed that the main northward flow in the Chukchi Sea was a coastally trapped current which directed to the Beaufort Sea (Sverdrup, 1929; LaFond and Pritchard, 1952; Paquette and Bourke, 1974) before 1975. Based on direct current measurements and variations of ice extent (Paquette and Bourke, 1981; Ahlnas and Garrison, 1984), this basin-scale flow pattern of the three main branches gradually becomes clear: one exists east to Hanna Shoal feeding into Barrow Canyon, one exists west to Herald Shoal which converges toward Herald Valley, and the third branch referred to as the Central Channel flow is located between the two shoals mentioned above. Compared to extensive research of flows in Barrow Canyon and Herald Valley, the direct measurements in the central channel are relatively sparse, therefore, the results from a few data show inconsistent and even opposite (Coachman *et al*., 1975; Weingartner *et al*., 1998). Based on a year-long current meter record in the central channel, a mean northward flow has been evidently observed (Weingartner *et al*., 1998), which is in contrast to the southward flow inferred by Coachman *et al*. (1975), and some observations also suggest a eastward flow occasionally present on the outer shelf of the Chukchi Sea (Johnson, 1989; Münchow *et al*., 2000). More interestingly, a new pathway for exchanges between the Chukchi Sea and the Arctic Ocean is observed feeding into the Long Strait along with these three main outflow branches from the Chukchi Sea (Woodgate *et al*., 2005),

* Corresponding author. Tel: 0086-532-88965239
E-mail: liun@fio.org.cn

which all suggest that the patterns of flow in the Chukchi Sea need to be further studied with the emphasis on the details in the central channel.

Tides in coastal and semi-enclosed seas are generally more difficult to predict and model than those in the deep ocean. Previous studies indicated that tides in the Chukchi Sea plays an important role in the distribution of ocean temperature, salinity and circulation by observations and numerical models (Cartwright, 1979; Pearson *et al.*, 1981; Kowalki, 1999; Foreman *et al.*, 2006). In addition to the effects of tides described above, recent studies demonstrated that tides can substantially impact the ice motion by amplifying the effect on the annual cycle of sea-ice formation and melting, although the tides in the Chukchi Sea are rather small (Woodgate *et al.*, 2005). Knowledge of tides and current in the central Chukchi Sea is not only critical to understand regional physical dynamics and ecosystem function (Day *et al.*, 2013), but particularly, a key point to support commercial fishing, oil spill trajectory surveying and new shipping routes exploring. Much of our understanding of tide characteristics in this area mainly derives from previous studies and indicates complicated distributions of semi-diurnal and diurnal tides (Li *et al.*, 2005; Wang *et al.*, 2011); however, the detailed features remain largely unknown.

Compared with active observations performed by American and Russian, the Chinese Arctic Research Expedition (CARE) was carried out relatively late but has developed rather quickly since its first cruise in 1999. Several short-time of moored observations were accomplished in the Chukchi Sea and its adjacent marginal sea during subsequent two CARE activities (Jiao *et al.*, 2008; Chen *et al.*, 2013). Considering the impact of tides and currents on the physical environment and dynamics processes, a new sub-surface mooring system was deployed during the 5th CARE in 2012. The present study focuses on the time series of ADCP measurements, with emphasis on the analysis of dominant tides components and residual currents in 2012 summertime. Although it only furnishes a short-term length of data, this work indicates a remarkable ~10 d variability which is closely related to the local wind forcing and allows us considering future mooring system configurations. Section 2 describes the system configuration and data retrieved. Section 3 analyzes the characteristics of several dominant tidal constituents existing in the central Chukchi Sea. Section 4 studies the profile of residual currents and examines their relationship to the local winds.

2 Measurements

To further advance our understanding of the characteristics of the short-term variability in the central Chukchi Sea, an upward-looking 300 kHz ADCP mooring was deployed at 69°30.155′N, 169°00.654′W (Fig.1), where the ADCP was mounted at ~20 m above seabed to avoid potential risks from the heavy ice expansion and fishing activities. The sampling interval was set to 20-minute, averaging 50 pings at 24-s, and hourly data was then obtained by averaging three samples. The vertical profile was binned using 2-m interval from the depth of the ADCP transducer up to the surface. However, because the surface layer data for depth shallower than 5 m were heavily contaminated by the signals reflected at the surface, only the data between 5 m and 37 m were analyzed in the present study. The mooring system was deployed on July 21 and recovered on September 8, 2012; hence a time series of 49-day data was collected. The short gaps in the data were linearly interpolated in time. In addition to the above measurements, variables of temperature and salinity across our selected time period were also obtained by 5 RBR CTD recorders mounted at different layers above the ADCP. The pressure data recorded by the CTD located 1 meter above ADCP was used to calibrate its depth variation and no significant change in the depth was indicated due to the swings of the mooring line.

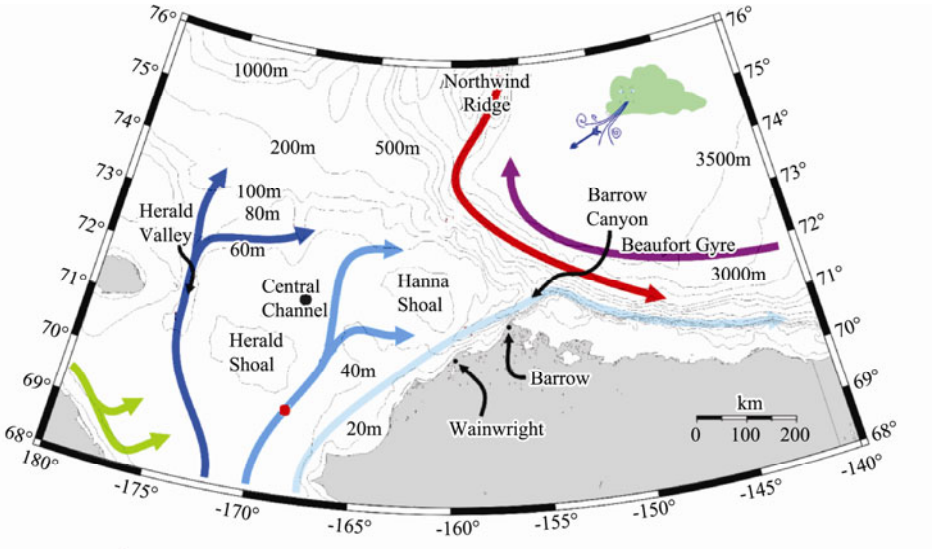

Fig.1 Bathymetric map of the Chukchi Sea showing the mooring positions (black dot and red dot indicate the positions of moorings deployed in 2008 and 2012, respectively. The base map is cited from http://www.ims.uaf.edu/chukchi).

3 Tidal Currents

To detect the dominant frequencies in current variations, a rotary spectral analysis is performed. Figs.2b, c and d show the power spectrum distributions of raw current at depths of 5, 21 and 37 m, corresponding to the typical depths of the surface layer, midlevel and deep layer, respectively, obtained from the CTD profile casted at 69°36.11′N, 168°51.72′W, where is much close to this mooring position. In addition to the local inertial frequency of 12.8 h, two other notable oscillations of proximate 12 h and 10 d are all evidently demonstrated in those three layers. Further more, both the oscillations have comparative amplitude and indicate that the tidal signals should be considered carefully.

A classic harmonic tidal analysis package (Foreman, 1978) is used for tidal analyses. Because of the relatively short measurement durations, only the dominant tidal constituents are analyzed using a given Rayleigh resolution criterion for least-square fit (Rayleigh constant is set to be 1.0). Applying this criterion, the largest 6 individual tidal constituents of M_2, S_2, N_2, O_1, MM, and MSF are well resolved for the mooring location; current amplitudes for these constituents as a function of depth are shown in Fig.3.

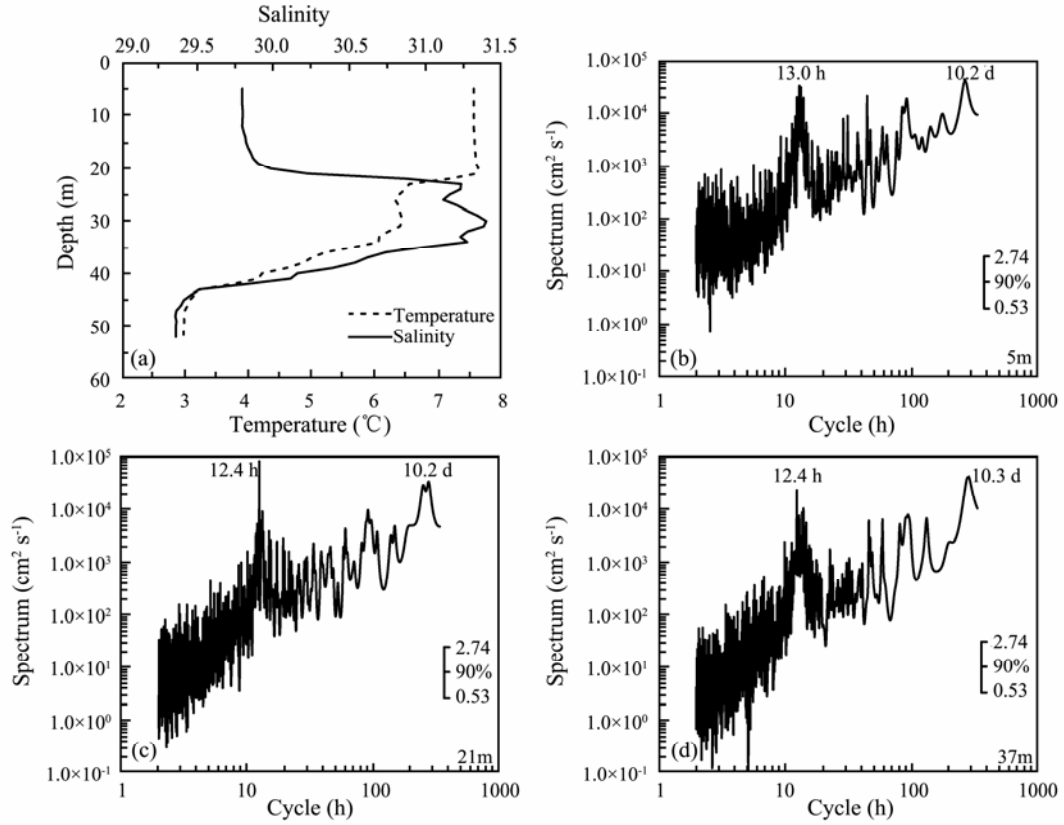

Fig.2 The profile of temperature (dashed) and salinity (solid) nearby the mooring (a) and power spectrum of current velocities at 5, 21 and 37 m.

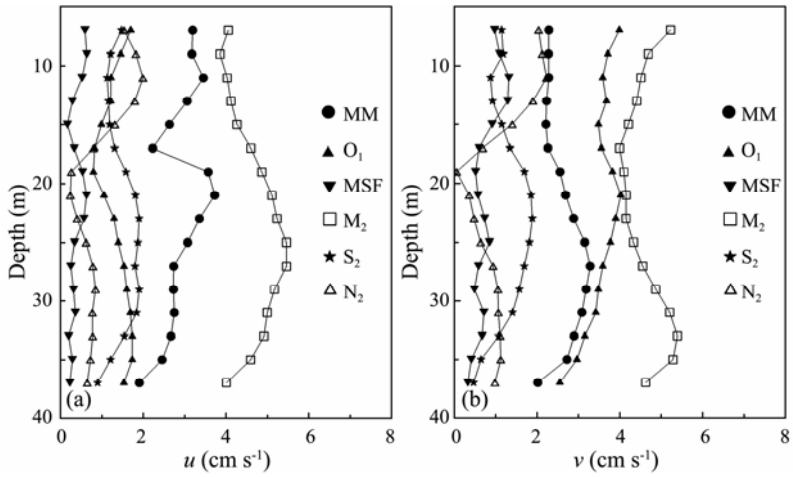

Fig.3 Amplitudes for individual tidal constituents (MM, O_1, MSF, M_2, S_2 and N_2) for *u* and *v* velocity components.

Among these resolved tidal constituents, M_2 current amplitudes of the *u* and *v* components are the largest throughout the water column with significant variations over depth; for depth-averaged tidal current series, the ratios of this tidal constituents to the total tidal current are 54% and 47% for *u* and *v* components, respectively. The M_2 current amplitudes of the *u* components are weaker (< 4.1 cm s^{-1}) at the upper levels than at midlevel (5.6 cm s^{-1} at 25 m depth), whereas the situations for the *v* component are the opposite to the above, *i.e.*, larger at the upper levels with maximum of 5.2 cm s^{-1} and minimum of 4.0 cm s^{-1} occurring at 17 m depth. The current amplitudes of *u* components for MM and N_2 have obvious variability in the upper layers; meanwhile, the current amplitudes of *v* components for MM appear more stable than N_2. In comparison, the current amplitudes of *u* components for MSF, O_1 and S_2 are relatively independent of the depth and generally have values smaller than 2 cm s^{-1}. The mean magnitude of depth-averaged tidal currents is about 15% of the original current magnitudes from the result of the harmonic tidal analysis. In other words, tidal currents are remarkably weaker and residual currents dominate, the latter being nearly 85% of the flows at this mooring position in the summer of 2012.

Major and minor semi-axes, inclination angles (semi-major axis rotation measured in degrees counterclockwise from the east) as a function of depth of the analyzed 6 tidal constituents are shown in Fig.4. The sign of the minor axis indicates the sense of rotation: positive implies counterclockwise rotation and negative implies clockwise rotation. All these chosen tidal constituents rotate clockwise throughout the water column with exception of MM and O_1. The largest two components of M_2 and S_2 are similar in eccentricity and orientation in deeper levels, but the magnitudes of the former are larger than the later. The magnitudes of minor semi-axes for M_2 and S_2 are more than twice as large as MM and MSF, while their major semi-axes are relatively comparable. Current ellipses for

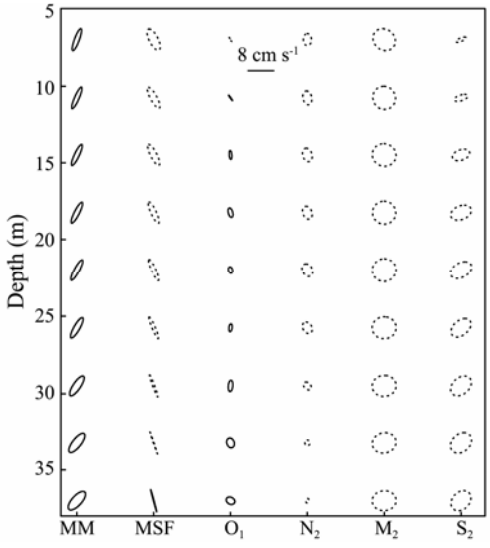

Fig.4 Current ellipses individual tidal constituents (solid line indicates counterclockwise rotation, dash line indicates clockwise rotation).

O_1 and N_2 are generally smaller and the ratio of major to minor semi-axis shows more depth-dependent than the other analyzed constituents. The ratio for O_1 is maximal 13.01 at 5 m and decreases over depth with minimal value 4.2 at a deeper level of 37 m; in contrast, the situations for N_2 for N_1 are completely reversed, where the ratios of minimum (~1.92) and maximum (~3.2) occur at 5 m and 37 m, respectively. In addition, the rotations for the above two tidal components are opposite, that is, O_1 rotates anti-clockwise while N_2 indicates clock-wise rotation.

4 Temporal and Vertical Structures of the Residual Current

The data are edited to eliminate spikes, being rotated by 5° to correct for the magnetic deviation from true north, and low-pass filtering using a Cosine-Lanczos filter with a 40-h cutoff is applied to remove tidal and other high frequency variations to obtain the residual currents. In order to better analyze the distribution characteristics of current velocity within the entire observed water column, current statistics for the tide-removed data consisting of mean current components, standard deviations, minimums, maximums, mean speed and directions (0° is north) are shown in Table 1. The maximum of residual currents varies in a range of 20–30 cm s^{-1} with depth, meanwhile, the maximum of *u* component (20.2 cm s^{-1}) is found in the upper layer and the minimum of 6.1 cm s^{-1} at the deepest bin (37 m). The variation for *v* component is similar to that for *u* component and the respective maximum and minimum are 21.9 cm s^{-1} and 16.0 cm s^{-1}. The vertical variation for mean *u* and *v* components duplicates the same trend at depths where $\overline{v}$ is significantly larger than $\overline{u}$, whereas σ_v is smaller than σ_u, suggesting that *v* components appear more stable throughout the observed water column during observation. Overall, the mean speed is relatively small (< 7 cm s^{-1}) and flowing toward the north.

Considering the depth and settings of ADCP, together with the vertical distribution of residual currents, the residual are shown in Fig.5, meanwhile, the time series of currents are compared with sea winds at the grid point closest to this mooring site from NOAA/NCDC Blended 0.25-degree Sea winds dataset (Zhang *et al*., 2006). The temporal resolution of currents and winds is 2 h and 6 h, respectively. It is obvious that currents in the upper levels are influenced greatly by the sea meteorological condition and its fluctuations. Currents in the surface layer (5 m) respond quickly to the winds and tend to flow north with southerly winds and to flow south with northerly winds. This variation of time series illustrates much difference to the previous observation in the summer of 2008 (Wang *et al*., 2011), in which the surface currents flow southward, being opposite to the southerly prevailing winds, and direction reverses at depths. On the other hand, both the currents variation suggest the complicated responses to the varying atmospheric and wind effects existing in the central Chukchi Sea, and the difference also results from two moorings with a distance larger than 2 meridional degrees between them (see Fig.1). The currents in

the deeper levels are toward relative true north and have mean velocities of approximately 5.4 cm s^{-1}. Near the end of the observation period, the strongest northeasterly burst was measured, and both the surface and deep layers responded to a strong northeastward flow of ~30 cm s^{-1} at ~1 day phase lag behind the winds.

Table 1 Statistics of ADCP records after tide-removing

Depth (m)	$\overline{u}$ (cm s^{-1})	σ_u (cm s^{-1})	u_{max} (cm s^{-1})	u_{min} (cm s^{-1})	$\overline{v}$ (cm s^{-1})	σ_v (cm s^{-1})	v_{max} (cm s^{-1})	v_{min} (cm s^{-1})	$\overline{S}_p$ (cm s^{-1})	*Dir* (°)
5	−2.1	11.2	20.2	−32.0	6.5	8.5	21.9	−19.9	6.9	342.4
7	−2.4	10.6	19.2	−33.1	6.4	8.0	21.4	−18.2	6.8	339.5
9	−2.5	9.8	17.1	−32.6	6.2	7.6	20.7	−16.9	6.7	338.2
11	−2.4	9.1	15.4	−30.9	6.3	7.6	20.6	−15.9	6.7	339.5
13	−2.3	8.5	13.5	−27.9	6.4	7.5	20.2	−16.8	6.8	340.5
15	−2.1	7.8	12.1	−23.7	6.5	7.3	21.0	−14.7	6.9	341.9
17	−1.9	7.2	10.9	−20.0	6.6	7.1	21.8	−14.1	6.9	343.9
19	−1.6	6.5	10.2	−17.9	6.6	7.3	22.4	−15.1	6.8	346.0
21	−1.4	5.9	10.1	−17.1	6.4	7.7	22.8	−19.7	6.6	347.8
23	−1.1	5.4	9.1	−16.9	6.2	7.9	21.9	−22.2	6.3	349.6
25	−0.9	5.1	7.9	−16.0	5.9	7.9	20.4	−22.6	6.0	351.1
27	−0.7	4.7	7.0	−14.2	5.7	7.9	19.3	−21.2	5.7	353.0
29	−0.7	4.6	6.6	−13.6	5.5	7.9	18.6	−21.3	5.5	353.2
31	−0.6	4.7	6.4	−13.6	5.4	8.1	18.7	−21.7	5.4	353.5
33	−0.5	4.7	6.6	−12.9	5.3	8.0	19.1	−21.6	5.3	354.8
35	−0.5	4.5	6.3	−12.3	5.3	7.7	18.7	−21.0	5.3	355.0
37	−0.4	3.8	6.1	−11.4	4.8	6.8	16.0	−21.2	4.8	355.7

Notes: $\overline{u}$ and $\overline{v}$ represent east-west and north-south components of velocity, respectively; $\overline{S}_p$, current speed; *Dir*, current direction (where 0° is north).

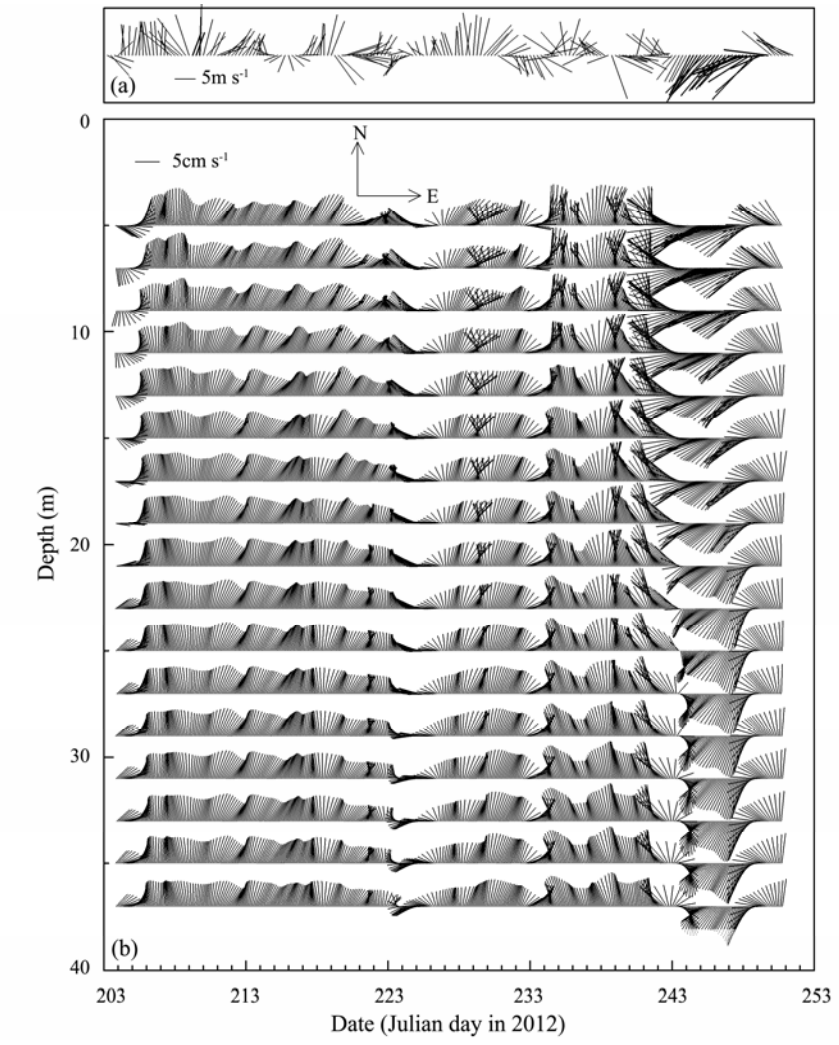

Fig.5 Vector-stick diagrams of wind speed and residual current velocities at different depth: (a) Wind speed at 10 m; (b) Residual current velocity.

The residual currents vary over depth and time, changing their directions nearly every 10 days, particularly significant variations in current magnitudes and directions occur firstly in the upper layer from Julian Day of 203 (August 8th), then propagate downward to deeper layer two days later. Strongest currents (~35 cm s^{-1}) occur at a shallow level near the surface (7 m bin). These currents measured in shallow levels are turning clockwise within nearly one-third of the record along with magnitudes decrease and directions well homogeneous over depth, with a generally northward flow throughout the whole observed water column in accordance with the southerly prevailing winds. A low-frequency fluctuation of the currents could be seen at a period of about 10 days.

Fig.6 (a) shows the time-averaged currents over depth in the observation period in 2012. As the most striking feature, the mean currents are all seen to be directed to the north throughout the whole observed water column, whereas the mean currents at 5 m in 2008 summer time flow toward the east-southeast. This implies that a stable northward current indeed exists in the central Chukchi Sea during 2012 summer time and even its depths are within the reach of the influence of the atmosphere. Meanwhile, the strongest currents occur at the upper levels (6.9 cm s^{-1} at 5 m) where the averaged direction points to NNW, and the weakest at the observed deepest leval (4.8 cm s^{-1} at 37 m) with the currents flowing more northward. Compared with the observation at 71˚40.024′N, 167˚58.910′W mentioned above in 2008 summertime, the mean currents in 2012 flow more true north with quite considerable magtitudes. In contract to the results of previous observation in the central Chukchi Sea (Li *et al*., 2005), the mean current in the deepest layer is chosen for this purpose. The magtitudes of mean current at 37 m in 2012 and that at 32 m in 2008 are 4.8 cm s^{-1} and 3.7 cm s^{-1}, respectively, while somewhat smaller magtitude of 1.3 cm s^{-1} at 38 m is observed at 70˚30.899′N, 167˚58.499′W in 2003 summertime, indicating that the northward flow in central Chukchi Sea is relatively weak but of high variability. The reason for the variability might be related to topographic difference between the two sites.

To quantify the influence of the northward flow on water properties in the central Chukchi Sea, the tide-removed current at 35 m is selected with corresponding to the temperature and salinity time series in the same layer as shown in Fig.7. It is notable that the currents and T-S are incoherent. However, some of the current variations coincide with the significant T-S fluctuations, which is probably caused by the passage of an upwelling event occurring along the northwestern Alaskan coast; this topic will be further studied with other supplementary data.

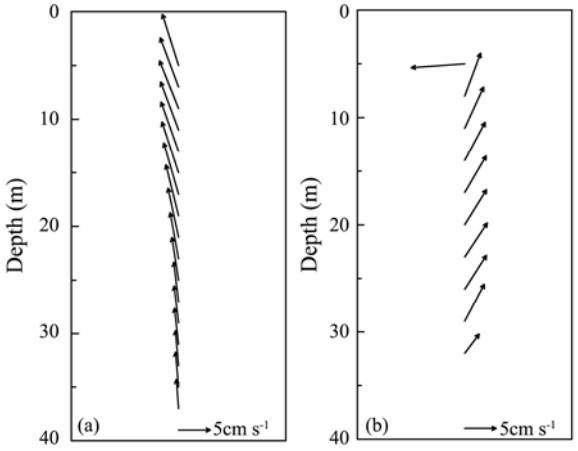

Fig.6 Observed mean residual currents over depth in 2012 (a) and 2008 (b).

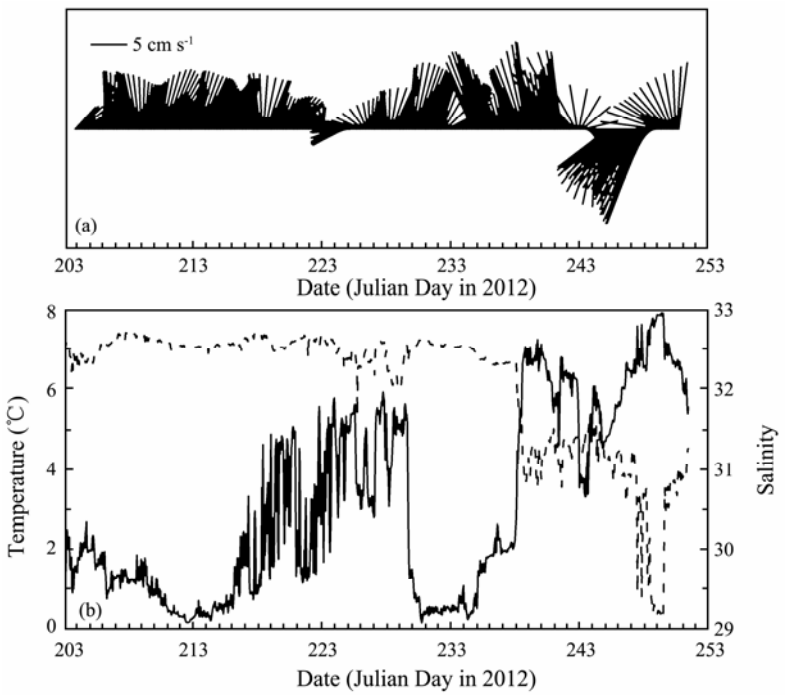

Fig.7 Residual current , temperature (solid), and salinity (dashed) time series at 35 m during 2012 summertime.

5 Cross-Spectral Analyses of Currents and Winds

For quantitatively comparing of the currents and the winds, spectra were computed for the meridional component, which all showed maxima in bands covering about 10 days period. Overall energy is higher in the surface layer currents than that in midlevel. The variability at the 10 d band implies a link between the local winds forcing and the currents.

To further understand the low-frequency fluctuation of the currents and its relationship with winds, the method of cross-spectral analyses is conducted. Considering the major characteristic of the prevailing winds during this observation, only the meridional components of the winds are applied for analyses. Fig.8 showed the squared coherence and phase lag between meridional currents and wind components at three different bins (5 m, 19 m and 37 m) with 95% confidence level, where negative phase lag means that winds lead currents.

Significant coherence (>0.8) is found between north-south components of currents and winds for 10 d period at 5 m (Fig.8a), and the phase of 54° corresponds to currents trail winds by ~1.4 d. Similar results are obtained at 19 m and 37 m, where the phase lag is ~1.6 d and ~1.7 d, respectively. These results suggested that the 10 d fluctuation of the currents is in response to fluctuation in the winds with response time of ~1.4 d, while the response at deep layer is several hours later than that at upper layer.

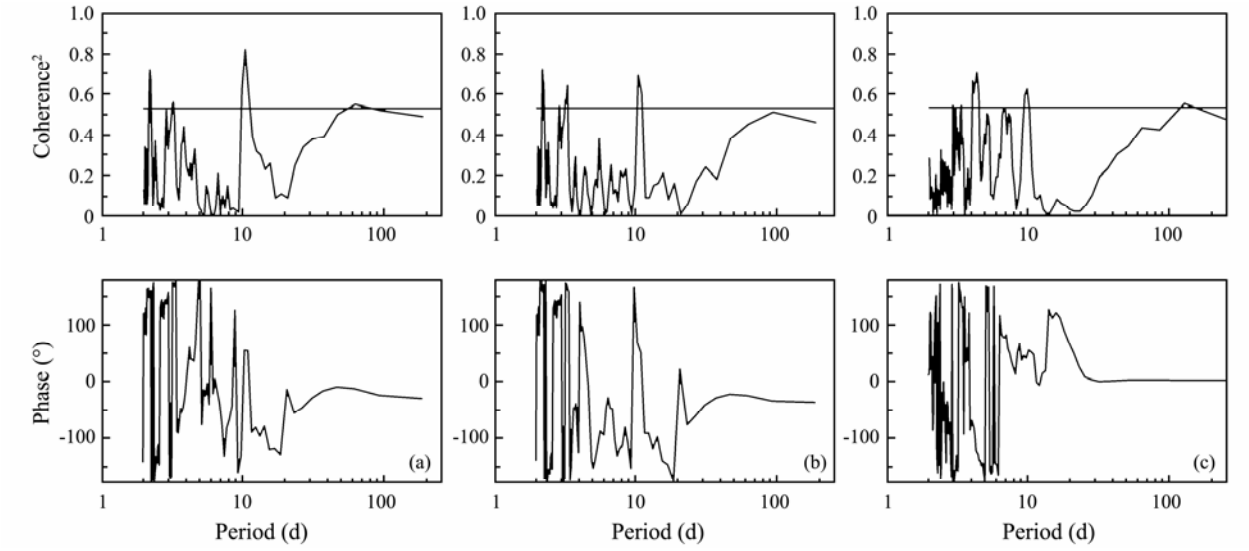

Fig.8 Coherence and phase diagrams for the meridional residual current and wind at: (a) 5 m; (b) 19 m; (c) 37 m. The 95% confidence level is indicated. Negative phase indicates that the current trails the wind.

6 Summary and Conclusion

During the mooring observation in the central Chukchi Sea, obvious high-frequency periodical fluctuations of the studied currents are attributed to semidiurnal tidal currents. The M_2 constituent is largest both in *u* and *v* components over depth, and followed by MM in *u* component and O_1 in *v* component, respectively. For depth-averaged tidal current series, the ratios of M_2 constituent current to the total tidal current are 54% and 47% for *u* and *v* components, respectively. All the resolved tidal constituents rotate clockwise throughout the water column with exception of MM and O_1. Both M_2 and S_2 are similar in eccentricity and orientation at deeper levels, but the magnitude of M_2 is larger than that of S_2.

Residual currents are considerably variable in both magnitude and direction in the summer of 2012, whereas the variation trend is basically homogeneous over the whole depth. The range of maximum currents is found between 20 and 30 cm s^{-1} and mean currents are generally weaker than 7 cm s^{-1}. Furthermore, the *v* component is much stronger than *u* component with similar tendency in standard deviation over depth. Time series of the residual currents exhibits poor coherence with the corresponding T-S at 35 m, while some of the current variations coincide with the larger T-S variations due to the possible passage of a front or eddy during the observation. Residual currents respond to meridional winds at a significant period of about 10 d with an approximately 1.4 d of response time at the 5 m depth, meanwhile, the currents at midlevel (19 m) and deeper level (37 m) have close response times 1.6 d and 1.7 d, respectively. Overall, local winds forcing appears to be the dominant driving mechanism and needs to be observed in future work.

Acknowledgements

Thanks are to the colleagues who participated in the deployment and recovery of the mooring system, including people from the First Institute of Oceanography, Ocean University of China, *R/V Xuelong*, and others. The authors would like to acknowledge the anonymous reviewers for their careful review and constructive com-

ments. This work is funded by the Basic Research Fund Project (GY2007T08), Public Science and Technology Research Funds Projects of Ocean (201205007-1), Chinese Polar Environment Comprehensive Investigation & Assessment Programmes (CHINARE-2014-03-01), and the Polar Science Strategic Research Foundation of China under contract No. JD201101.

References

Ahlnas, K., and Garrison, G. R., 1984. Satellite and oceanographic observations of the warm coastal current in the Chukchi Sea. *Arctic*, **37**: 244-254.

Arrigo, K. R., Perovich, D. K., Pickart, R. S., Brown, Z. W., Van Dijken, G. L., Lowry, K. E., Mills, M. M., Palmer, M. A., Balch, W. M., Bates, N. R., Benitez-Nelson, C. R., Brownlee, E., Frey, K. E., Laney, S. R., Mathis, J., Matsuoka, A., Mitchell, B. G., Moore, G. W. K., Reynolds, R. A., Sosik, H. M., and Swift, J. H., 2014. Phytoplankton blooms beneath the sea ice in the Chukchi Sea. *Deep-Sea Research II*, **105**: 1-16.

Cartwright, D. E., 1979. Analysis of British Antarctic survey tidal records. *British Antarctic Survey Bulletin*, **49**: 167-179.

Chen, H. X., Wang, H. W., Shu, Q., Wang, D. L., and Liu, N., 2013. Ocean current observation and spectrum analysis in central Chukchi Sea during the summer of 2008. *Acta Oceanologica Sinica*, **32** (3): 10-18.

Coachman, L. K., Aagaard, K., and Tripp, R. B., 1975. *Bering Strait, the Regional Physical Oceanography*. University of Washington Press, 172pp.

Coachman, L. K., and Aagaard, K., 1966. On the water exchange through Bering Strait. *Limnology and Oceanography*, **11**: 44-59.

Day, R. H., Weingartner, T. J., Hopcroft, R. R., Aerts, L. A. M., Blanchard, A. L., Gall, A. E., Gallaway, B. J., Hannay, D. E., Holladay, B. A., Mathis, J. T., Norcross, B. L., Questel, J. M., and Wisdom, S. S., 2013. The offshore northeastern Chukchi Sea, Alaska: A complex high-latitude ecosystem. *Continental Shelf Research*, **67**: 147-165.

Foreman, M. G. G., 1978. Manual for tidal currents analysis and prediction. *Pacific Marine Science Report*, **1**: 70.

Foreman, M. G. G., Cummins, P. F., Cherniawsky, J. Y., and Stabeno, P. J., 2006. Tidal energy in the Bering Sea. *Journal of Marine Research*, **64**: 797-818.

Hunt, G. L., Blanchard, A. L., Boveng, P., Dalpadado, P., Drinkwater, K. F., Eisner, L., Hopcroft, R. R., Kovacs, K. M., Norcross, B. L., Renaud, P., Reigstad, M., Renner, M., Skjoldal, H. R., Whitehouse, A., and Woodgate, R. A., 2013. The Barents and Chukchi seas: Comparison of two Arctic shelf ecosystems. *Journal of Marine Systems*, **109-110**: 43-68, DOI: 10.1016/j.marsys.2012.08.003.

Jiao, Y. T., Zhao, J. P., Shi, J. X., Wu, W., and Zhang, H. X., 2008. Design and deployment of anchorage surveying system in Polar region. *Ocean Technology*, **29** (1): 53-60.

Johnson, W. R., 1989. Current response to wind in the Chukchi Sea: A regional coastal upwelling event. *Journal of Geophysical Research*, **94**: 2057-2064.

Kowalik, Z., 1999. Bering Sea tides. In: *The Bering Sea: Physical, Chemical and Biological Dynamics*. Alaska Sea Grant Press, 93-127.

LaFond, E. C., and Pritchard, D. W., 1952. Physical oceanographic investigations in the eastern Bering and Chukchi seas during the summer of 1947. *Journal of Maine Research*, **11**: 69-86.

Li, L., Du, L., Zhao, J. P., Zuo, J. C., and Li, P. L., 2005. The fundamental characteristics of current in the Bering Strait and Chukchi Sea during July to September 2003. *Acta Oceanologica Sinica*, **24** (6): 1-11.

Münchow, A., Carmack, E. C., and Huntley, D. A., 2000. Synoptic density and velocity observations of slope waters in the Chukchi and East-Siberian Seas. *Journal of Geophysical Research*, **105**: 14103-14119.

Paquette, R. G., and Bourke, R. H., 1974. Observations on the coastal current of arctic Alaska. *Journal of Marine Research*, **32**: 195-207.

Paquette, R. G., and Bourke, R. H., 1981. Ocean circulation and fronts as related to ice melt-back in the Chukchi Sea. *Journal of Geophysical Research*, **86** (4): 4215-4230.

Pearson, C. A., Mofjeld, H. O., and Tripp, R. B., 1981. Tides of the eastern Bering Sea shelf. In: *The Eastern Bering Sea Shelf: Oceanography and Resources*. Calder, J. A., and Hood, D. W., eds., University of Washington Press, 111-130.

Roach, A. T., Aagaard, K., Pease, S. A., Weingartner, T. J., Pavlov, V., and Kulakov, M., 1995. Direct measurements of transport and water properties through Bering Strait. *Journal of Geophysical Research*, **100**: 18443-18457.

Sverdrup, H. U., 1929. The waters on the north Siberian shelf. *Scientific Research of the Norwegian North Polar Expedition*, **4**: 1-131.

Walsh, J. J., McRoy, C. P., Coachman, L. K., Goering, J. J., Nihoul, J. J., Whitledge, T. E., Blackburn, T. H., Parker, P. L., Wirick, C. D., Shuert, P. G., Grebmeier, J. M., Springer, A. M., Tripp, R. D., Hansell, D. A., Djenidi, S., Deleersnijder, E., Henriksen, K., Lund, B. A., Andersen, P., Muller-Karger, F. E., and Dean, K., 1989. Carbon and nitrogen cycling within the Bering/Chukchi Seas: Source regions for organic matter effecting AOU demands of the Arctic Ocean. *Progress in Oceanography*, **22**: 277-359.

Wang, H. W., Chen, H. X., Lv, L. G., and Wang, D. L., 2011. Study of tide and residual current observations in Chukchi Sea in the summer 2008. *Acta Oceanologica Sinica*, **33** (6): 1-8 (in Chinese).

Weingartner, T. J., Cavalieri, D. J., Aagaard, K., and Sasaki, Y., 1998. Circulation, dense water formation and outflow on the northeast Chukchi Sea shelf. *Journal of Geophysical Research*, **103**: 7647-7662.

Woodgate, R. A., Aagaard, K., and Weingartner, T. J., 2005. A year in the physical oceanography of the Chukchi Sea: Moored measurements from autumn 1990–91. *Deep-Sea Research II*, **52**: 3116-3149.

Zhang, H. M., Reynolds, R. W., and Bates, J. J., 2006. Blended and gridded high resolution global sea surface wind speed and climatology from multiple satellites: 1987–present. *American Meteorological Society 2006 Annual Meeting*, Paper P2.23.

(Edited by Xie Jun)